ECTI Transactions on Computer and Information Technology
Journal homepage: https://ph01.tci-thaijo.org/index.php/ecticit/
Published by the ECTI Association, Thailand, ISSN: 2286-9131

Multicarrier Modulation Schemes for 5G Wireless Access

Abu Shakil Ahmed[1], Husam Al-amaireh[2] and Zsolt Kollár[3]

ABSTRACT

The 5G wireless access technology will supersede its predecessor, 4G, in the current decade, at first coexisting with it and later as a standalone technology. This work examines and compares the performance of the following orthogonal multicarrier schemes: Cyclic Prefix Orthogonal Frequency Division Multiplexing (CP-OFDM), Windowed Orthogonal Frequency Division Multiplexing (W-OFDM), Filtered Orthogonal Frequency Division Multiplexing (F-OFDM), Universal Filtered Multi-Carrier (UFMC), and Filter Bank Multi-Carrier (FBMC). The system architecture of each scheme is investigated while considering the performance in fading channel models. The simulation was performed using a standard set of parameters, and the performance was appraised based on Power Spectral Density (PSD), Peak to Average Power Ratio (PAPR), Complementary Cumulative Distribution Function (CCDF) of PAPR, Bit Error Rate (BER), and Signal to Noise Ratio (SNR). In addition, a comprehensive analysis is presented concerning filter or window implementation, filtering method, orthogonality, roll-off rate, spectral leakage, spectral efficiency, computational complexity, and runtime complexity. Based on the results, each scheme has its advantages and disadvantages compared with the other methods. FBMC, F-OFDM, and W-OFDM are preferred for better spectrum utilization, transmission accuracy, and power efficiency, respectively. UFMC offers a fine balance between these multicarrier schemes. Therefore, the modulation scheme for the future physical layer will strongly depend on the requirements.

Article information:

Keywords: Multicarrier Modulation, 5G, Physical layer, CP-OFDM, W-OFDM, F-OFDM, UFMC, FBMC

Article history:
Received: June 10, 2022
Revised: July 12, 2022
Accepted: August 20, 2022
Published: September 24, 2022 (Online)

DOI: 10.37936/ecti-cit.2022164.248710

1. INTRODUCTION

Several multicarrier modulation schemes have been proposed for the physical layer of wireless access technology, and all have pros and cons [1]. Numerous studies of the candidate modulation schemes have been performed, most of which compare a limited number of modulation schemes. However, to fully explore the potential of 5G, a more in-depth comparison between the schemes is needed. For example, each modulation scheme can use various filtering/windowing methods that may impact the performance. Furthermore, transmission media characteristics play a vital role in signal propagation.

Many authors have conducted comparison studies among multicarrier schemes. In [2], a survey on the waveforms for 5G was presented that included a comparison among Cyclic Prefix Orthogonal Frequency Division Multiplexing (CP-OFDM), Filtered Orthogonal Frequency Division Multiplexing (F-OFDM), Filter Bank Multi-Carrier (FBMC), Generalized Frequency Division Multiplexing (GFDM), and Universal Filtered Multi-Carrier (UFMC). The schemes were compared based on the filter granularity, time and frequency orthogonality, out-of-band emission, latency, and robustness against carrier frequency offset. The scope of comparison can be extended by adding several other important performance parameters such as spectral efficiency, spectral leakage, spectral resolution, and Peak to Average Power Ratio (PAPR). In [3], the performance of multicarrier waveforms was reported with a comparison

[1]The author is with Graduate Student Member, IEEE, ORCID: 0000-0001-8075-1733, E-mail: shakil.ahmed.bd71@gmail.com
[2]The author is with Department of Broadband Infocommuncations and Electromagnetic Theory, Budapest University of Technology and Economics, 1111 Budapest, Hungary, E-mail: husam.alamaireh@gmail.com
[3]The author is with Department of Measurement and Information Systems, Budapest University of Technology and Economics, 1111 Budapest, Hungary, ORCID: 0000-0001-6384-265X, E-mail: kollarzs@mit.bme.hu
[1]Corresponding Author.

among FBMC, UFMC, GFDM, Resource Block F-OFDM (RB-F-OFDM), and OFDM, mainly for 5G asynchronous communications based on the nonlinearity of high-power amplifiers, multi-user interference, numerical complexity, and spectral efficiency. Although this analysis is more extensive than the previous approach, the inclusion of a good channel model and different undesired effects on the signal can improve the study. Moreover, the performance of multiple channel models can be tested as well. In [4], UFMC was implemented. Its performance was compared with OFDM and FBMC waveforms to justify its effectiveness for different applications of 5G, including the internet of things (IoT) and user-centric signal processing of communication systems. The authors concluded that UFMC offered better spectral efficiency and robustness than OFDM and better burst transmission than FBMC. However, the scope of comparison can be extended, and some other prominent schemes can be included to offer a broader comparison. In [5], the FBMC scheme's performance was analyzed and compared with OFDM, UFMC, F-OFDM, and Weighted Overlap and Add OFDM (WOLA-OFDM) schemes. The study emphasized the effectiveness of FBMC over the other multicarrier schemes. FBMC was implemented using a polyphase network (PPN), and the channel model was designed for multipath propagation. The performance was evaluated based on the relationship between Bit Error Rate (BER) and Signal to Noise Ratio (SNR). Here, the number of performance parameters can be increased, and the channel models may be extended. In [6], the performance and complexity of OFDM, FBMC, UFMC, and GFDM were evaluated to assess their prospect as 5G waveform contenders. The comparison was conducted based on PAPR, Power Spectral Density (PSD), spectral efficiency, multiplication per symbol, and robustness to multiple users for the uplink scenario. Two test implementations of FBMC were presented. The study suggested that FBMC was the most prominent modulation scheme for the 5G physical layer. The work can be extended by enhancing the channel model and considering unwanted phenomena that degrade the signal on different occasions. In [7], another comparative study was reported on OFDM, FBMC, and UFMC waveforms based on PSD and spectral efficiency. Moreover, the effect of filter length, overlapping factor, and burst transmission were observed on these schemes. It was suggested that UFMC provided better performance for burst transmission, and higher spectral efficiency, and that lower interference was achieved in FBMC. However, other well-known schemes, such as Windowed OFDM (W-OFDM), F-OFDM, and GFDM, can be incorporated into the study. Also, important performance analyses such as the Complementary Cumulative Distribution Function (CCDF) of PAPR and BER-SNR relationship can be included. Furthermore, a good channel model is needed to determine the performance of the schemes more precisely.

In [8], the performance of Full Duplex FBMC (FD-FBMC) was examined, considering it as a solution for the full-duplex multicarrier scheme for cellular systems. The performance of the OFDM system was reported in terms of spectral leakage interference. Moreover, the improvement of this parameter was investigated while using other multicarrier modulation schemes such as FBMC, UFMC, GFDM, and F-OFDM. Their findings showed that FBMC is the best scheme among them for the suppression of spectrum leakage. In conclusion, it was reported that the degradation was still considerable in other schemes though the improvement was more noticeable than that of OFDM. The model is simplistic and can be expanded.

In [9], the green coexistence among the candidates of the 5G waveform was reviewed, incorporating multicarrier schemes such as OFDM, F-OFDM, GFDM, UFMC, and FBMC. The performance was evaluated based on PAPR, computational complexity, spectral efficiency, latency, and filter length. It was reported that FBMC and UFMC offered more promising coexistence with OFDM than other approaches. However, the novelty of other multicarrier modulation schemes needs to be explored more. Also, the channel model needs to be expanded, including different undesired effects on the signal caused by the filtering effects of the channel.

In [10], the authors compared Multiple Input Multiple Output (MIMO) systems using OFDM, UFMC, and FBMC as the modulation schemes. Their performance was assessed based on BER, PSD, data rate and spectral confinement. It was reported that UFMC offered the highest data rate, whereas FBMC offered the finest PSD. Although MIMO systems were included in the analysis, the number of performance metrics was limited. Therefore, the comparison could be extended by including more parameters.

In [11], a comparative study was performed, including OFDM, F-OFDM, UFMC, FBMC, and GFDM modulation schemes. Their performance was compared in terms of spectral efficiency, complexity, out-of-band emission, adjacent band interference, side lobe attenuation, and time-frequency efficiency. However, the channel model can be added and extended. Besides, the depth of analytical and simulation assessment can be enhanced. Based on the above discussion, analysis needs to be performed on the various modulation schemes with variations in their implementations, such as type and length of the windows and filters, order of symbol mapping, channel models, and equalization techniques.

Overall, the performance of the transceiver units of the modulation schemes can be evaluated based on several performance metrics such as PSD, BER,

SNR, PAPR, and CCDF of PAPR. As a function of frequency, PSD indicates the distribution of the whole signal over the frequency spectrum and gives a sense of bandwidth-neutral constant signal amplitude [12]. BER evaluates the accuracy of data transmission. It can be lowered by decreasing the bandwidth, increasing the transmission power, and using a lower order modulation scheme, which causes a reduction in throughput, increase in power consumption, and decrease in spectral efficiency [13]. Multicarrier modulation schemes concede high PAPR for signal transmission, and a High Power Amplifier (HPA) with a sizeable linear region is needed to avoid distortion [14]. Lastly, CCDF is an important parameter to monitor how long the signal remains above a specific PAPR value. [15].

Most comparisons reported in the literature deal with two modulation schemes. On the other hand, the majority of the extended studies are based on standard implementations of modulation schemes. The selection of different parameters contributes to the overall effectiveness of each modulation scheme. For example, each modulation scheme may use different filtering methods, the characteristics of which differ significantly. There are also windowing techniques, whose response varies from one to another. The characteristics of the transmission medium between the transmitter and the receiver also play an important role in signal propagation. Therefore, a more elaborate review is a necessity to fully explore the potential of 5G. This study presents a comprehensive comparative assessment incorporating the following modulation schemes: CP-OFDM, W-OFDM, F-OFDM, UFMC, and FBMC. The performance is appraised based on a wide range of matrices such as PSD, PAPR, CCDF of PAPR, BER, SNR, filtering method, orthogonality, roll-off rate, spectral leakage, spectral efficiency, computational complexity, and runtime complexity. All transceiver units are designed considering both fading and nonfading channel models to evaluate the effect of the undesirable artifacts. Moreover, the simulation is performed using a common set of parameters to offer a fair comparative assessment. The aim is to provide a guideline for selecting modulation schemes according to the requirements.

The manuscript is arranged into five sections. Besides the introduction in section I, the architectures of the multicarrier modulation schemes are presented in section II. Then in section III, we have reported the simulation outcomes and commented on their technical aspects. Next, a comparative analysis is offered in section IV. Finally, section V contains the conclusion of the report.

2. MULTICARRIER MODULATION SCHEMES

The principal characteristic differences among the schemes are the filtering and windowing processes. While CP-OFDM is implemented without any filter, W-OFDM is designed with a window and F-OFDM with a lowpass Finite Impulse Response (FIR) filter. Different types of filters are chosen for UFMC and FBMC. Next, we will briefly discuss each multicarrier scheme and then study their performance.

2.1 CP-OFDM

As a multicarrier scheme, each sub-carrier of CP-OFDM has a low bit rate and, therefore, the signal is quite long in the time domain, making it robust towards multipath fading [16]. Furthermore, since the sub-carriers are orthogonal relative to each other, they are overlapped, keeping the spacing the same as the inverse of the symbol period between two consecutive carriers. Notably, every symbol is spread among a set of subcarriers so that the symbols are spaced in time [17]. In this way, the onset of a burst error may be prevented in signal transmission. However, any unwanted nonlinearity in the system impairs the orthogonality and creates interference due to intermodulation distortion [18].

The design of the CP-OFDM modulation scheme is relatively more straightforward than other schemes. First, the input data or binary bitstream is processed using a symbol mapper such as Quadrature Amplitude Modulation (QAM) to increase the number of bits per symbol, resulting in increased spectral efficiency. QAM combines amplitude and phase modulation to encode the signal in log2 M number of bits per symbol, where M indicates the number of constellation points in the IQ plane [19]. Then, the modulated complex signal is oversampled by zero padding. We placed the zeros initially on either side of the signal and then shifted them in the middle [20]. Next, the signal is transformed into a time-domain through the Inverse Fast Fourier Transform (IFFT) operation. After that, a Cyclic Prefix (CP) is attached to the beginning of each symbol. Finally, the OFDM symbols are generated by implementing IFFT as per (1), and CP is inserted [21].

$$\mathrm{x[n]} = \frac{1}{N}\sum_{k=0}^{N-1}\left[X[k]e^{\frac{j2\pi kn}{N}}\right], \quad n = 0, 1, 2, \ldots N-1 \quad (1)$$

Here, x[n] is the OFDM signal in the discrete-time domain, k is the index of IFFT bins, and N is the total number of IFFT bins. The architecture of the CP-OFDM transmitter is presented in figure 1.

The sequence of the signal recovery process is almost the reverse of the signal transmission. The transmitted signal experiences some filtering effect in the channel and becomes noisy. Therefore, the received signal is equalized in the frequency domain

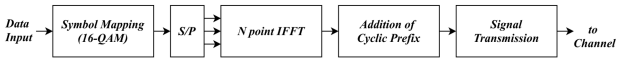

Fig.1: *Block Diagram of the CP-OFDM Transmitter*

to neutralize the unwanted channel effects. We used Zero Forcing Equalizer (ZFE) when either of the fading channel models, Rayleigh or Rician, is considered. Notably, transmission through a nonfading channel model with only AWGN requires no symbol elongation and equalization [22]. The complete signal reception process is illustrated graphically in figure 2 [23].

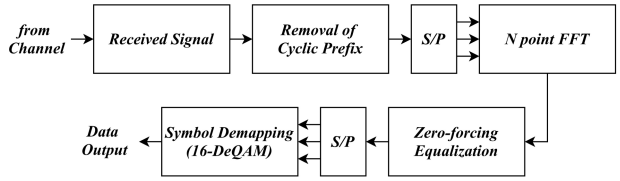

Fig.2: *Fig.2: Block Diagram of the CP-OFDM Receiver.*

2.2 W-OFDM

One of the most unfavorable aspects of OFDM is its spectral leakage. A fraction of the signal power gets leaked into undesired frequency bins in this case. Besides, when a symbol period starts and ends with discontinuous amplitudes, it makes the approximation of Fast Fourier Transform (FFT) difficult [24]. Windowing techniques can help to reduce the spectrum and alleviate the problem, although they cannot eliminate it. Thus, a window function is applied to the OFDM signal before transmission. The rest of the signal processing steps are the same as CP-OFDM [25].

As stated, a window function reduces the remote band noise by decreasing the discontinuity between successive OFDM symbols to achieve a smooth transition. However, it creates some distortion in the signal, although it is negligible and depends on the window size [25]. If the length of the window increases in the time domain, its resolution decreases. In contrast, it has the opposite effect in the frequency domain, where the resolution increases. Therefore, higher frequency resolution translates to lower signal distortion. On the other hand, a short-length window function increases the resolution in the time domain, reducing the resolution in the frequency domain and further distorting the signal [26]. At the receiver, the time-domain signal is returned to the frequency-domain by the FFT operation. A window function is usually symmetrical and has a maximum amplitude at its midpoint, which gradually reaches zero towards the edges governed by the characteristics of the window [27].

In this study, we used a raised cosine window function. The description of the window in the frequency domain is expressed in (2), where N_{sym} is the number of symbols and T_{sym} stands for the symbol period. The relationship between the roll-off rate β and the excess bandwidth Δf is indicated in (3) [28].

$$H(f) = \begin{cases} 1, |f| \leq \frac{1-\beta}{2T} \\ \frac{1}{2}\left[1+\cos\left(\frac{\pi N_{sym}}{\beta}\left[|f| - \frac{1-\beta}{2T}\right]\right)\right], \frac{1-\beta}{2T_{sym}} < |f| \leq \frac{1+\beta}{2T_{sym}} \\ 0, else \end{cases} \quad (2)$$

$$\beta = \frac{\Delta f}{\left(\frac{1}{2T_{sym}}\right)} = 2T_{sym}\Delta f \quad (3)$$

A raised cosine window shapes the symbols individually, i.e., the extension of a symbol is multiplied by the window function in the time domain. In contrast, the original symbol is not affected by the window. The resultant symbol amplitude approaches zero near the start and the end [27]. Thus, the spectral leakage is reduced. Finally, the signal is transmitted through the channel. The transmitter architecture of the W-OFDM modulation scheme is shown in figure 3 [29].

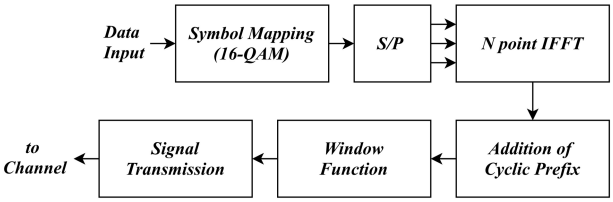

Fig.3: *Block Diagram of the W-OFDM Transmitter.*

The signal recovery process is like CP-OFDM. Initially, the symbols are shrunk back to their original length by removing the CPs [21]. After that, the time-domain signal is reverted to the frequency-domain by taking out data from OFDM symbols by applying FFT [30]. At this point, the channel effects are mitigated by equalization, which is ZFE in this case. The architecture of the W-OFDM receiver used in this study is shown in figure 4 [31].

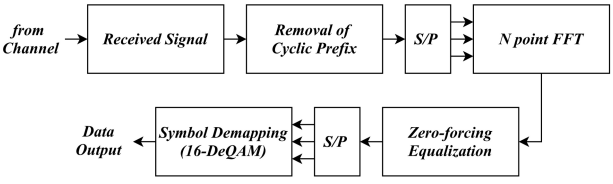

Fig.4: *Block Diagram of the W-OFDM Receiver.*

2.3 F-OFDM

Another approach to improve the spectral efficiency of the CP-OFDM multicarrier scheme is the

usage of filters. A filter is applied to the signal produced by the CP-OFDM scheme immediately before the transmission. Hence, the filter is placed at the very end of the CP-OFDM transmitter architecture. Since the signal is in the time domain, the filter is also designed in the time domain. Filtering helps to keep the out-of-band radiation at a minimum [32].

A good filter should have three essential characteristics. First, the filter's passband needs to be uniform over the range of subcarriers so that the intended section of the signal can be transmitted through the channel. Second, the size of the guard bands needs to be decreased, and hence the transition band should be sharp enough. Third, it should provide sound stopband attenuation, keeping the width of the side lobes shorter [33]. The F-OFDM scheme applies a filter on all the subcarriers together. We chose a low pass FIR filter as the prototype in this study. It is designed by truncating the sinc function by a Hanning window. The smoothing process simplifies the transitions to zero at the end of the filter. The Hanning window is defined in (4), where L denotes the length of the window [34].

$$\omega_0(x) = \begin{cases} \frac{1}{2}(1+\cos(\frac{2\pi x}{2})), |x| \leq \frac{L}{2} \\ 0, |x| > \frac{L}{2} \end{cases} \quad (4)$$

The passband of the filter determines the bandwidth of the transmitted signal. Since the transition band is not perfectly sharp in practice, several subcarriers adjacent to the edge might be affected. However, the length of the filter is often allowed to surpass the length of CP, ensuring the number of the affected subcarriers is negligible. Otherwise, Intersymbol Interference (ISI) may occur [32]. Usually, the length of CP is adjusted to mitigate this adversity. Figure 5 shows a graphical representation of the F-OFDM transmitter [35].

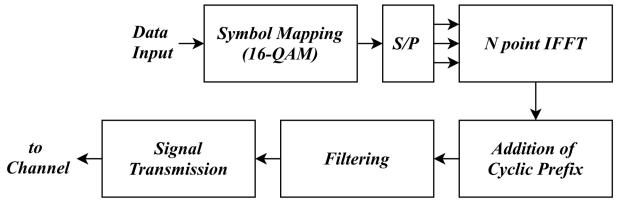

Fig.5: *Block Diagram of the F-OFDM Transmitter.*

F-OFDM has a similar signal recovery process as a variant of the CP-OFDM modulation scheme except for an additional step for inverse filtering. Here, after the removal of CPs, the filtering effect at the receiver is canceled out by applying a matching filter, i.e., a clone of the filter used at the transmitter end [21]. In addition, the delay caused by the filtering is mitigated. Next, N point FFT is performed for unpacking OFDM symbols [30]. After that, equalization is performed to counteract the fading effect that occurred in the channel [22]. Finally, the output bitstream is obtained by symbol demapping. The architecture of the F-OFDM receiver is presented in figure 6 [35].

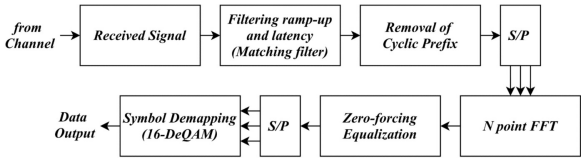

Fig.6: *Block Diagram of the F-OFDM Receiver.*

2.4 UFMC

Universal Filtered Orthogonal Frequency Division Multiplexing (UF-OFDM) or UFMC is another variant of OFDM that is also a practical multicarrier modulation scheme for the 5G physical layer. It is an approach halfway between F-OFDM and FBMC because, unlike F-OFDM, the subcarriers are filtered group-wise, whereas, in FBMC, they are filtered individually. The subcarrier groups are called subbands and can be filtered using either a different filter for each subband or the same filter for all [36].

The filter length is considerably lower in UFMC concerning F-OFDM since it is performed at the subband level. Like F-OFDM, filtering is performed to minimize the out-of-band radiation so that leakage suppression can improve spectral efficiency [36]. In this study, we used the Dolph-Chebyshev filter, and the same filter is applied for each subband. This filter minimizes the main lobe width according to a preset sidelobe attenuation. Moreover, the filter exhibits equiripple characteristics because the sidelobes have the same height in the frequency domain. On the other hand, it gives impulses at the endpoints in the time domain. A couple of parameters define the filter during the implementation: filter length and side lobe attenuation. The filter is described in (5), where T_N denotes the Chebyshev polynomial of the first kind [37].

$$\omega_0(k) = \frac{T_N(\beta\cos(\frac{\pi k}{N+1}))}{T_N(\beta)} = \frac{T_N(\beta\cos(\frac{\pi k}{N+1}))}{10^{\alpha}}, 0 \leq k \leq N \quad (5)$$

Initially, the total available band is split into subbands containing several subcarriers. Then the data bits are divided among them and mapped separately using a symbol mapper [19]. The mapped symbols are padded with zeros to fit the signal to the size of IFFT, and then zeros are shifted in the middle of the signal. Next, the IFFT is implemented on each sub-band to assign the QAM symbols to the bins [30]. After that, the time-domain subband signals are filtered using the Dolph-Chebyshev filter. In this study, we used ten subbands, and the processing was done in parallel for each of them. The UFMC signal generation process is illustrated in figure 7 [38].

The receiver architecture is significantly different

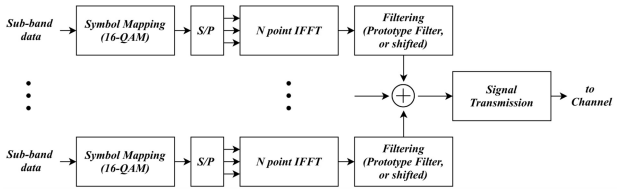

Fig.7: *Block Diagram of the UFMC Transmitter.*

in UFMC than in the already discussed schemes. First, the received signal is upsampled by zero paddings for fitting it to the next FFT size [20]. Then the complex time-domain samples are converted back to the complex samples in the frequency-domain using a double-sized FFT [30]. Subsequently, the signal is downsampled to restore the signal length. The block diagram of the signal recovery process at the UFMC receiver end is shown in figure 8 [38].

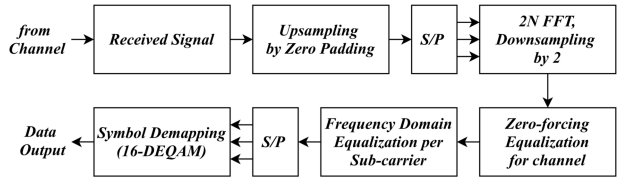

Fig.8: *Block Diagram of the UFMC Receiver.*

2.5 FBMC

FBMC is another multicarrier modulation scheme and a promising candidate for the physical layer of 5G and beyond. Besides reduced spectrum efficiency, the users of original OFDM systems also need strict synchronization. FBMC can handle these two issues efficiently [39]. As an illustration, a subcarrier level filtering process in FBMC makes the system robust against ISI. Hence, the symbols do not need to be extended using CP that increases the usable spectrum [40].

The filter coefficients define the prototype filter, and the number of coefficients depends on the overlapping factor, K. Thus, the overlapping factor characterizes the prototype filter. Here, the overlapping factor denotes the number of symbols that overlap in the time domain within a single symbol period [39]. In this work, we have chosen a Phydyas prototype filter. The frequency coefficients can be calculated using (6), and the corresponding impulse response of the prototype filter follows (7), where Hk denotes the set of filter coefficients, L indicates the filter length, and N implies the number of subcarriers [41]. Finally, the filter order is set by 2K-1, where K ranges from 2 to 4.

$$H(f) = \sum_{k=-(K-1)}^{K-1} H_k \frac{\sin(\pi(f - \frac{k}{NK})NK)}{NK \sin(\pi(f - \frac{k}{NK})NK)} \quad (6)$$

$$h(t) = 1 + 2\sum_{k=1}^{K-1} H_k \cos\left(2\pi \frac{kt}{KT_{sym}}\right) \quad (7)$$

Like the UFMC scheme, the transmitter architecture in FBMC is different from that of OFDM systems. First, Offset Quadrature Amplitude Modulation (OQAM) is used instead of QAM. Secondly, the OQAM modulated signal spreads to K times the number of subcarriers in the frequency domain [42]. However, the system complexity increases since the Fourier transformation computationally becomes more complex. In this way, the IFFT block may retain its size simply by adjusting the overlapping factor even though the number of subcarriers is changed [43]. The frequency spreading process includes upsampling, insertion of guard bands, and application of the prototype filter. As the prototype filter coefficients are symmetric, fewer multiplications are needed. The extended IFFT transforms the complex signal to a complex time-series and shifts the zero-frequency component into the middle [44]. Finally, the delayed imaginary and real parts are summed together and transmitted through the channel. The FBMC transmitter architecture is illustrated in figure 9 [45].

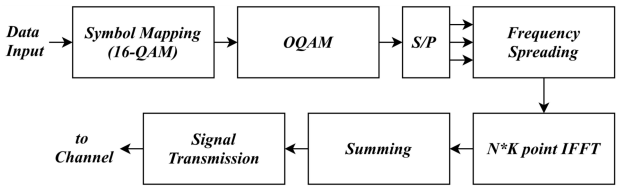

Fig.9: *Block Diagram of the FBMC Transmitter.*

The signal recovery process is the opposite of the transmitter end processing. First, the signal is transferred back to the frequency domain by extended FFT operation. Then, the received signal is equalized to offset the channel effect. Subsequently, the filtering effect at the transmitter end is balanced using a matching filter. Since the guard bands are of no use now, they are removed from the signal, and the extended signal is downsampled to restore the original length. At this stage, the interleaved real and imaginary parts of the signal are joined together by OQAM post-processing, and the complex signal is obtained [42]. Finally, the original bitstream is recovered by DeQAM symbol demapping. The signal processing steps at the FBMC receiver are illustrated in figure 10 [45].

3. SIMULATION OUTCOMES

The performance of each of the multicarrier modulation schemes was evaluated based on a set of performance metrics. In addition, the responses of different filters and window functions along with the channel

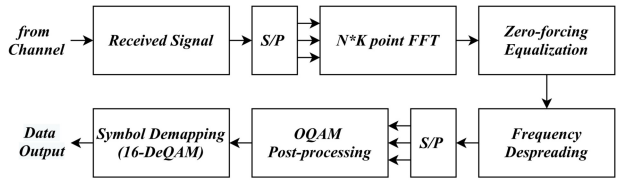

Fig.10: *Block Diagram of the FBMC Receiver.*

characteristics are presented graphically in this section. However, the goal of this study is to offer an extensive comparison based on the performance of the orthogonal multicarrier modulation schemes. For that reason, all schemes are simulated using a standard set of simulation parameters as specified in table 1.

Table 1: *Parameters of Multicarrier Schemes.*

Parameter	CP-FDM	W-OFDM	F-OFDM	UFMC	FBMC
subcarriers	512	512	512	512	512
resource blocks or sub-bands	20	20	20	20	N/A
subcarriers per resource blocks or sub-band	10	10	10	10	N/A
modulation scheme	16 QAM	16 QAM	16 QAM	16 QAM	16 QAM
symbols	100	100	100	100	100
overlapping symbols	N/A	N/A	N/A	N/A	4
cyclic prefix length	36	36	36	N/A	N/A
sub-band offset	N/A	N/A	N/A	156	N/A
guards on each side	N/A	N/A	N/A	N/A	156
tone offset in subcarriers	N/A	N/A	2.50	N/A	N/A
filter, window	N/A	raised cosine	Sinc function, Hanning window	Dolph-Chebyshev	Phydyas filter
filter or window length	N/A	36	257	43	K times FFT
SNR (dB)	17	17	17	17	17

Table 2: *Specification of Channel Models.*

Simulation Parameters	Rayleigh Channel	Rician Channel
Input signal sample rate (Hz)	10000	10000
Discrete path delay	5×10^{-7}	5×10^{-7}
Average gains of the discrete paths (dB)	0.50	0.50
Normalize average path gains to 0 dB	Yes	Yes
Rician K-factor	N/A	3
Maximum Doppler shift for all channel paths (Hz)	30	30

We used three different channel models: AWGN only, Rayleigh fading with AWGN, and Rician fading with AWGN. The multicarrier signal consists of a lot of carriers with reduced symbol rates. Since the parallel subchannels are narrowband and have lower data rate, the effect of fading on them can be considered to be flat instead of frequency selective. We set the path delay to a scalar value, 5x10-7 in this case. The average gain of the discrete paths in the channel is related to the path delay. It represents the number of discrete paths in the channel. The value is set to 0.50 in this analysis. The maximum Doppler shift is dependent on the input signal sample rate. The channel estimation and the synchronization are assumed to be perfect. The specification of the fading channel models is presented in table 2.

3.1 CP-OFDM

The success of signal transmission can be predicted by observing the constellation diagram at a glance. The constellation diagrams of the recovered symbols for AWGN, Rayleigh, and Rician channel models are presented in figure 11 for three different SNR values: 13 dB, 15 dB, and 17 dB. For AWGN, the constellation points fit the reference points nicely, and there is almost no deviation. Moreover, the constellation points are more scattered for Rayleigh than AWGN and Rician channel models. The fading effect plays a role in deviating the constellation points in Rayleigh and Rician channel models. Also, the absence of a dominant or Line-of-sight (LoS) propagation path is the reason behind the signal degradation in the Rayleigh channel model being worse than the Rician's. However, despite the displacement of the symbols on the I-Q plane, they form clusters around the corresponding reference points, and each cluster has significant separation from its neighbors. Besides, with the increase in SNR, the deviation decreases.

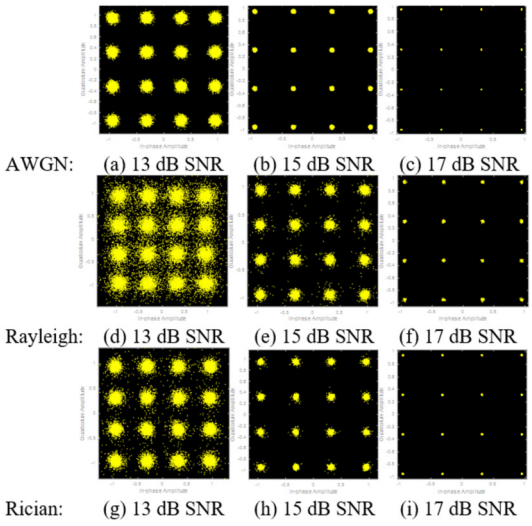

Fig.11: *CP-OFDM Constellation Diagram.*

3.2 W-OFDM

In this sub-section, we have presented the performance appraisal of W-OFDM like CP-OFDM. W-OFDM has one additional signal processing step: implementing a raised cosine window before the signal transmission. Therefore, the contribution of the window function is significant. The magnitude and the phase responses of the raised cosine window are presented in figure 12. Also, its impulse response in the overlapping region for both the rising and the falling edges is shown in figure 13. Here, the original symbols are multiplied by unit impulse responses, and are thus unaffected.

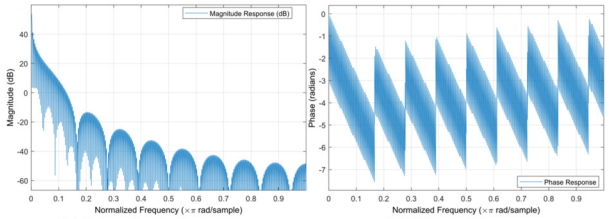

(a) Magnitude Response (b) Phase Response

Fig.12: *Magnitude and Phase Response of the Raised Cosine Window.*

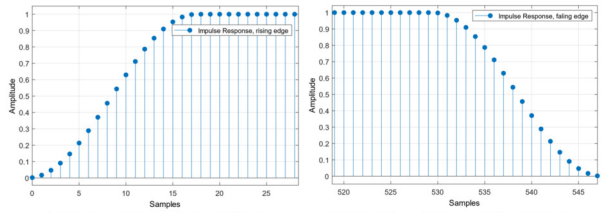

a) Rising Edge of the Window (b) Falling Edge of the Window

Fig.13: *Impulse Response of the Raised Cosine Window.*

After converting the time-series signal to the frequency-domain at the receiver end, the constellation diagram of the obtained W-OFDM symbols is presented in figure 14. It shows that the symbols are slightly less scattered than CP-OFDM. However, the difference is not so apparent as to be perceived by simple sight. The comparative figures are better for AWGN than for AWGN with the fading channel models.

3.3 F-OFDM

In the F-OFDM approach, we performed an additional filtering process instead of simply applying a window to scale the spectrum and remove a portion of it. Notably, the length of the filter used in F-OFDM is much higher than the tapering length of the window due to the bandwidth requirements. The low pass FIR filter is implemented along with a Hanning window to trim down its response after the cut-off frequency. The magnitude response presented in figure

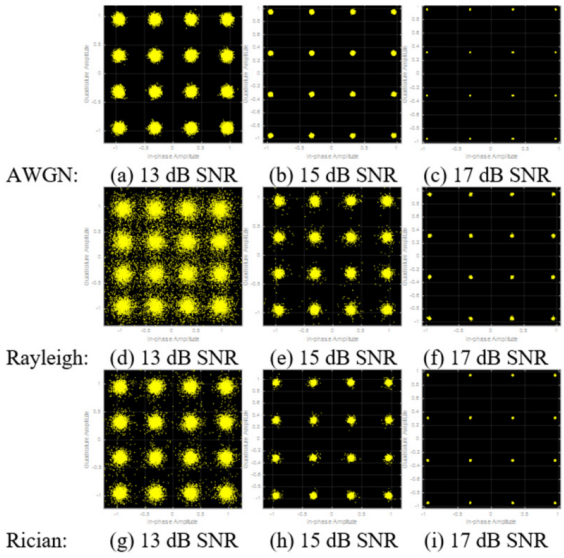

Fig.14: *W-OFDM Constellation Diagram.*

15 (a) suggests that the passband ripple is insignificant, the transition band is very slim, the stopband attenuation is slightly less than -100 dB, the normalized cut-off frequency is somewhat more than 0.4, and the stopband ripple is approximately 40 dB wide in magnitude. Figure 15 (b) shows that the phase response is linear for the passband 0 to 0.41π radian per sample and a small ripple is present in the stopband. It means all frequency bins should experience the same delay within this linear region and do not get distorted. The filter impulse response is shown in figure 16. We can observe the system characteristics in the time domain impulse response. Moreover, the filter length represents the spectral transition width of the filter, the main lobe width indicates the filter bandwidth, and the sinc function suggests it is an LPF.

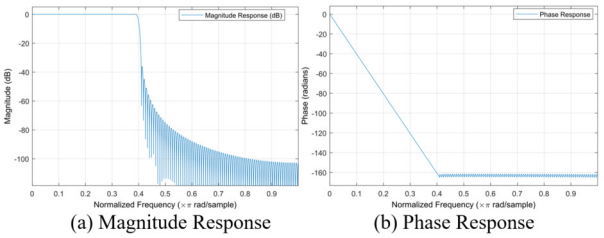

(a) Magnitude Response (b) Phase Response

Fig.15: *Magnitude And Phase Response of the Filter.*

The constellation diagrams for AWGN and fading channels with AWGN are shown in figure 17. The constellation points for the AWGN channel are apparently more degraded than the previous two modulation schemes. The other constellation diagrams are affected as well. However, the clusters around the reference points are well separable. In this case, the orthogonality of adjacent carriers is slightly lost

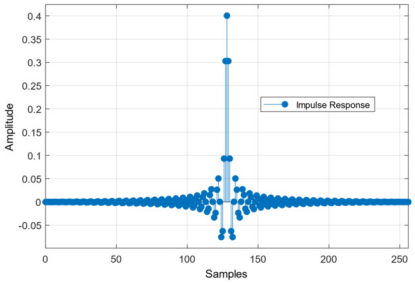

Fig.16: *Impulse Response of the Filter.*

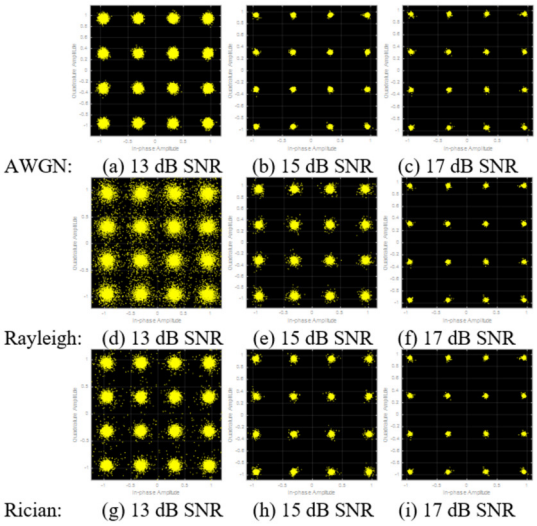

Fig.17: *F-OFDM Constellation Diagram.*

because the filter length is more than the CP.

3.4 UFMC

The main difference between the UFMC modulation scheme and the previous one is how filtering is performed. Unlike F-OFDM, the filtering is done on individual sub-bands instead of the whole band. In this study, we applied the Dolph-Chebyshev filter for each subband. Another critical point is that CP is not added to individual symbols. Instead, each sub-band is separated by a sub-band offset value. The filter's magnitude and phase responses are illustrated in figures 18 (a) and 18 (b), respectively, and the impulse response is shown in figure 19. As can be seen in the phase response, the filter has linear region from 0 to 0.09 π radian per sample. It is implemented by a convolution between the IFFT output and the filter's impulse response.

The constellation diagrams of the received signal for the UFMC scheme are presented in figure 20. As anticipated, the AWGN channel model has the most compelling constellation points. Despite the fading effect, the constellation diagrams of other channel models are also clear enough to distinguish the symbols.

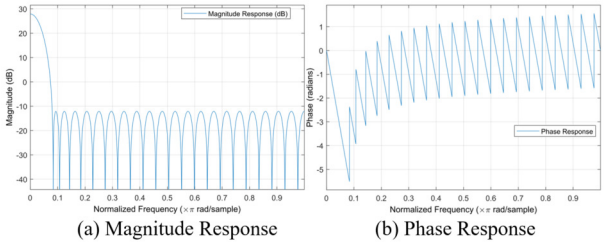

Fig.18: *Magnitude and Phase Response of the Dolph-Chebyshev Filter.*

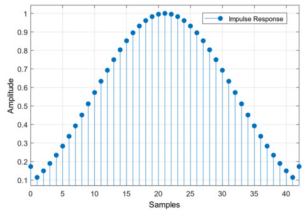

Fig.19: *Impulse Response of the Dolph-Chebyshev Filter.*

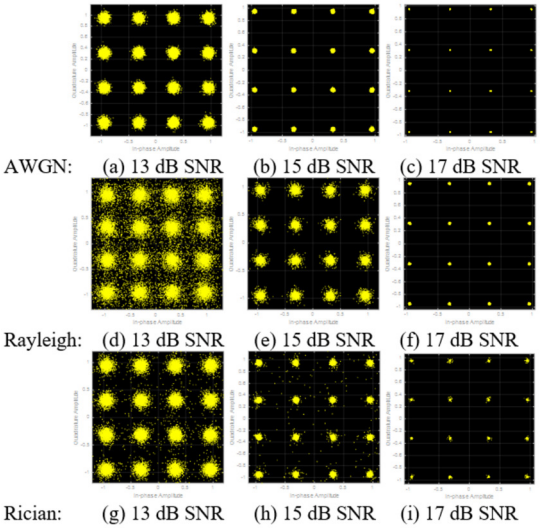

Fig.20: *UFMC Constellation Diagram.*

3.5 FBMC

Among the multicarrier modulation schemes discussed so far, FBMC uses the filters most extensively. Unlike F-OFDM and UFMC, each subcarrier is individually filtered in FBMC. We used a prototype filter from the Phydyas project with an overlapping factor of 4. Figures 21 (a) and 21 (b) indicate the magnitude and the phase responses of the filter, and the impulse response is presented in figure 22. We can observe in the phase plot that the filter has a large liner region from 0.04π to 0.99π radians per sample that effectively avoids distortion set off by high PAPR.

The 16-QAM symbols are nicely separated in the constellation diagrams shown in figure 23. It appears that both the Modulation Error Ratio (MER) and the

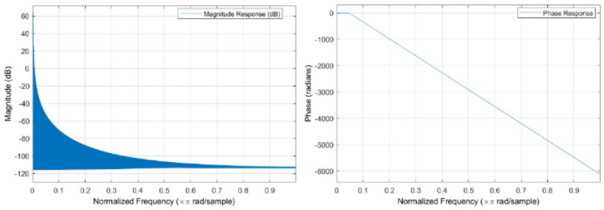

(a) Magnitude Response (b) Phase Response

Fig.21: *Magnitude and Phase Response of the Prototype Filter.*

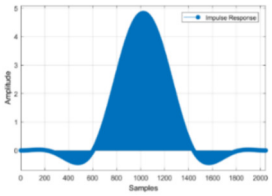

Fig.22: *The Impulse Response of the Prototype Filter.*

Quadrature Error (QE) are negligible. Moreover, the AWGN channel model offers the most commendable constellation diagram, followed by Rician.

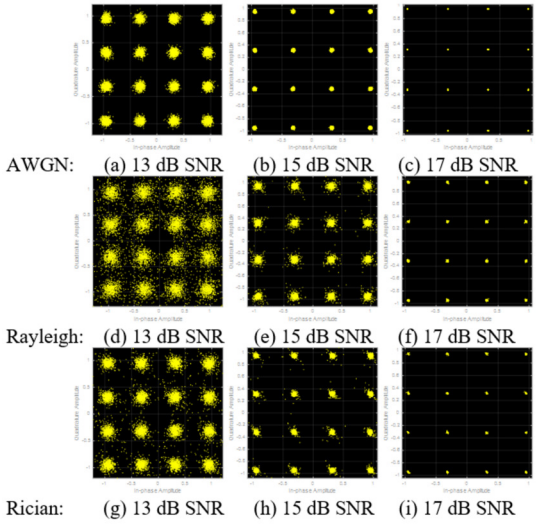

Fig.23: *FBMC Constellation Diagram.*

4. COMPARATIVE ANALYSIS

A comparative analysis is presented in this section, including the following performance metrics: filter or window used, filtering method, filter or window length, orthogonality, PAPR, CCDF of PAPR, BER, roll-off rate, spectral leakage, spectral efficiency, computational complexity, and runtime complexity. Finally, critical comments are offered based on the overall evaluation.

The PSDs of all the schemes are presented together in figure 24. The unit of PSD, in this case, is dBW/Hz, i.e., the power is expressed in dB, and it is normalized. There is a trade-off between leakage suppression and spectral resolution. The roll-off rate is not as high for CP-OFDM as for the others, suggesting insufficient spectrum leakage suppression. In addition, the sidelobe level is not considerably lower. Thus, a considerable amount of power is transmitted in the unused spectrum. The sidelobe level is lower in W-OFDM than CP-OFDM. Thus, W-OFDM offers better leakage suppression. In addition, the roll-off rate is visually higher, which indicates a rapid drop of PSD in the sidelobes. Therefore, the transmission power is conserved to some extent. As can be seen, the roll-off rate is higher in UFMC than both CP-OFDM and W-OFDM, though due to the equiripple characteristics of the Dolph-Chebyshev filter, the sidelobe level remains almost the same in UFMC.

Observing the PSD plot of F-OFDM, it is apparent that it offers considerably better leakage suppression than the earlier three schemes. Its sidelobe level is almost four times lower than CP-OFDM, nearly two times lower than W-OFDM, and significantly lower than UFMC. Therefore, the roll-off rate is improved, and spectrum efficiency is significantly higher. The PSD curve of FBMC is very promising. The roll-off factor is the highest, and the sidelobes are attenuated nicely, giving the lowest sidelobe level. Therefore, the spectrum leakage is negligible, and the spectrum efficiency increases. In total, CP-OFDM has the least roll-off rate, whereas FBMC has the highest, followed by F-OFDM, UFMC, and W-OFDM. Consequently, FBMC has the highest depth regarding the sidelobe level. Therefore, it offers the best leakage suppression among them.

As mentioned earlier, there is a trade-off between sidelobe attenuation and main lobe width. Thus, the number of subcarriers is kept the same for all schemes to better compare them with other multicarrier schemes, and the sidelobe attenuations are compared. Moreover, it helps to distinguish the closely spaced frequency components in all the schemes in the same way. Another critical point is that the PSD of the useful spectrum does not fluctuate significantly, indicating that the linear distortion is insignificant here. The observation is justified by a numerical comparison of the amplitude of PSD curves presented in table 3.

Table 3: *Comparison of Sidelobe Levels.*

Modulation Scheme	**PSD amplitude (dBW/Hz)**	**Normalized frequency**
CP-OFDM	-34.21	-0.50
W-OFDM	-80.46	-0.50
F-OFDM	-137.20	-0.50
UFMC	-73.34	-0.50
FBMC	-161.02	-0.50

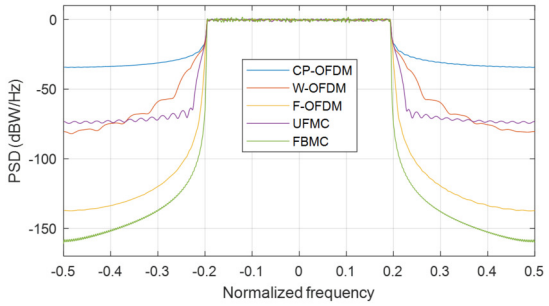

Fig.24: *Comparison of Power Spectral Density (PSD).*

The CCDF-PAPR relationship is also a critical aspect of the modulation schemes. It estimates the probability of PAPR exceeding the desired value and helps find the optimal range of variation in PAPR. The CCDF of PAPR is assessed by varying the number of symbols from 1 to 100, and the corresponding (CCDF, PAPR) pairs are captured. The relationship is plotted in figure 25, where the horizontal axis is scaled logarithmicly. In CP-OFDM, the CCDF decreases rapidly with the increase in PAPR. Then, the curve is slightly higher in the W-OFDM scheme for the same PAPR level than CP-OFDM, suggesting that the probability of PAPR having a value beyond the threshold is a bit higher in W-OFDM. On the other hand, F-OFDM concedes high PAPR, indicating that the possibility of exceeding the PAPR threshold is significantly higher. Therefore, an HPA with a larger linear region is needed for its implementation. The characteristic is better in UFMC than F-OFDM, though it is less promising than W-OFDM and CP-OFDM. It balances the CCDF of PAPR between non-filtered OFDM approaches and its filtered version. In this way, UFMC is a mid-way approach. Although FBMC is more promising than F-OFDM, its characteristics are less attractive than the rest. Altogether, we can see that F-OFDM can exceed the PAPR threshold more often than the other schemes, whereas CP-OFDM is the most energy-efficient scheme, and W-OFDM, UFMC, and FBMC are added to the sequence in turn.

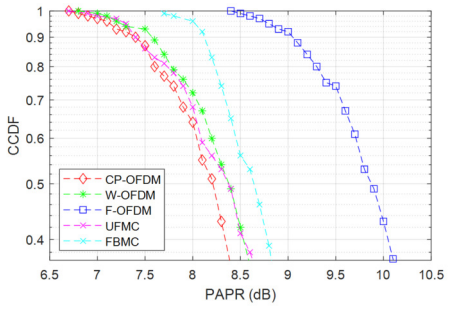

Fig.25: *Comparison of CCDF-PAPR Relationship.*

The comparative robustness of the modulation schemes against the noise effect is presented in figure 26, where the horizontal axis uses a logarithmic scale. Here the relationship between BER and SNR is presented separately for each channel model. The value of SNR varies from 1 dB to 16 dB, and the corresponding BER is recorded. Figure 26 (a) shows that CP-OFDM is the most vulnerable scheme against AWGN for an SNR within the specified range, whereas FBMC is the most robust. The BER-SNR curve of W-OFDM closely trails the CP-OFDM's, and the UFMC's and the F-OFDM's curves follow next in turn. In the case of Rayleigh fading with AWGN, F-OFDM surpasses CP-OFDM momentarily, whereas the other curves maintain their sequence, as shown in figure 26 (b).

The best to the worst BER-SNR relationship sequence under Rician fading with AWGN is CP-OFDM, W-OFDM, UFMC, F-OFDM, and FBMC, respectively are depicted in figure 26 (c). The error rate generally gets lowered in W-OFDM relative to the CP-OFDM approach due to the application of an additional window. Although windowing distorts the signal, the rising and falling edges are carefully applied to the extended parts of each symbol. Thus, the original symbols remain intact, and the transition between the consecutive symbols becomes smoother than CP-OFDM's. Due to the filtering, the transmitted signal becomes more robust in F-OFDM against the channel noise than both CP-OFDM and W-OFDM.

A similar phenomenon is observed in the case of UFMC. It offers lower BERs for corresponding SNRs for the AWGN channel, followed by the Rician and Rayleigh fading channels. Notably, FBMC is the best scheme in this assessment because of its filtering control at the subcarrier level. Overall, the signal gets distorted the most in Rayleigh fading, mainly because of the absence of a dominant path for signal propagation. Rician has less BER than Rayleigh because of the dominant path, while AWGN causes the least disturbance to the signal.

It is also convenient to estimate the runtime of each modulation scheme to gain insight into performance. Since all of them differ in their signal processing steps, this observation provides supplementary information about the prospect of choosing a modulation scheme. Therefore, we iterated the simulation of each modulation scheme six times and captured the last five runtimes to calculate the average. Figure 27 shows the normalized average runtime of the modulation schemes. Again, we can presume that FBMC takes the longest time to run, followed by F-OFDM and UFMC. Moreover, W-OFDM requires a little more time than CP-OFDM.

The computational complexity of each modulation scheme was evaluated using the MATLAB algorithm analyzer. Here, we observed the number of multipli-

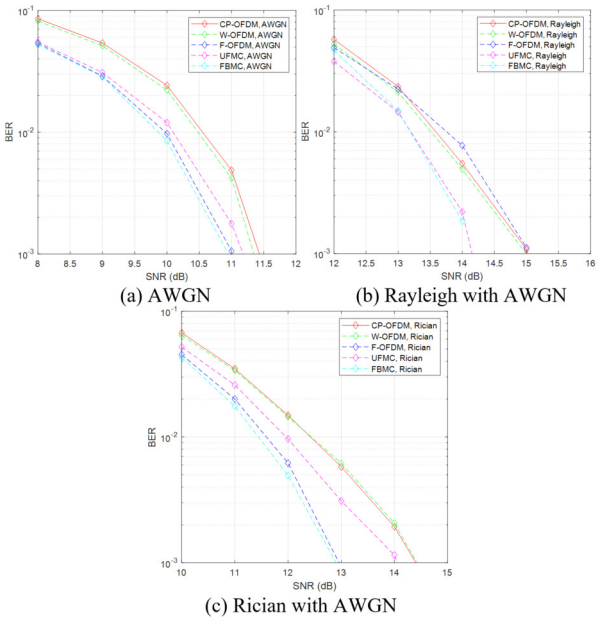

Fig.26: *Comparison of BER-SNR Relationship.*

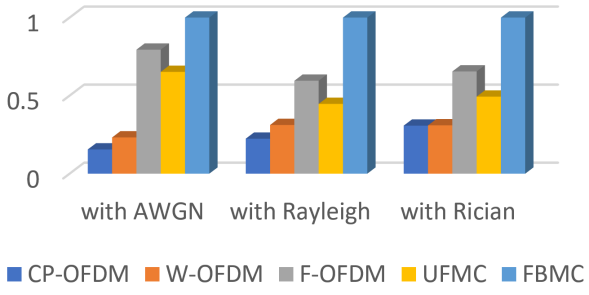

Fig.27: *The Normalized Runtime Complexity of the Modulation Schemes.*

cations and additions needed to implement the transmitter and receiver units and different channel models. A detailed analysis of the computational complexity of the selected modulation schemes is presented in table 4. The computational complexities of the transmitter and receiver units are added and then normalized relative to computationally the most expensive modulation scheme. UFMC is the most complex modulation scheme, followed by FBMC, F-OFDM, W-OFDM, and OFDM.

We have presented an overall observation on the performance of all four modulation schemes in table 5, considering their performance concerning all the performance parameters. In the final analysis, there is no single modulation scheme to prefer. The candidate modulation scheme can be chosen on every occasion as per the requirement. Nevertheless, if we prioritize PAPR, W-OFDM is preferred since it concedes less PAPR than other 5G modulation schemes. Again, FBMC is preferable for its spectral efficiency and transmission accuracy. Instead, we can use F-OFDM since it offers considerable transmission accuracy and leakage suppression, not to mention its ability to use CP that makes the symbols robust against multipath propagation. Above all, UFMC may perform as a mid-way approach since it balances the characteristics.

This study may be extended to include more modulation schemes, especially the non-orthogonal schemes. The reduction of PAPR can also contribute to this, which can increase the efficiency of the power amplifier [46]. In addition, it can be extended to the MIMO architectures and potential integrations of the enabling technologies, such as beamforming and millimeter waves, can enrich the system's capacity as a whole [47].

5. CONCLUSION

5G will replace 4G as the state-of-the-art wireless access technology in the current decade. However, no single modulation scheme proposed is a unanimously selected candidate scheme for the 5G physical layer. Therefore, a wide range of choice factors has been presented based on different performance metrics. The preferred scheme can be chosen considering the specific metrics according to requirements. W-OFDM, F-OFDM, UFMC, and FBMC can all utilize the available spectrum more efficiently than CP-OFDM. However, as shown in this study, they have different trade-offs to realize that.

W-OFDM focuses more on power efficiency and performs similar to CP-OFDM in several other metrics such as PAPR. At the same time, it decreases the sidelobe level and has a higher roll-off rate. Thus, it can suppress the out-of-band leakage more efficiently than CP-OFDM. Notably, this scheme does not significantly increase the computational complexity and runtime. We used raised cosine window to implement the W-OFDM modulation scheme. Again, filtering methods can suppress the out-of-band radiation more than using the windowing approach.

We can achieve much higher spectral efficiency in the F-OFDM scheme in exchange for more computational costs and less speed. In addition, the system becomes more robust against data loss. It requires more power consumption, and PAPR increases. Sinc filter with Hanning window was used for the filter design of F-OFDM. The filter is applied to the whole band altogether. Furthermore, we can increase spectrum efficiency and reduce BER to a greater extent with more comprehensive filtering approaches such as UFMC and FBMC. FBMC performs filtering at the subcarrier level. Thus, we can precisely control the emission of individual subcarriers. The PAPR and the system complexity go up as a trade-off. The prototype filter was designed using the coefficients of the Phydyas project. Alternatively, UFMC applies a filter on each sub-band and balances the spectrum utilization and the power requirement. However, this

Table 4: *Comparison on Computational Complexity.*

Channel	Transceiver	CP-OFDM	W-OFDM	F-OFDM	UFMC	FBMC
N/A	Transmitter (multiplication)	744845	745018	848278	44589343	2956406
	Transmitter (addition)	1582295	1582989	1793224	225377721	8470706
AWGN	Reciver (multiplication)	444836	444837	547748	35123	2904903
	Reciver (addition)	1543019	1542614	1747635	620036	8421202
	Σ multiplication	1189681	1189855	1396026	44624466	5861309
	Σ addition	3125314	3125603	3540859	225997757	16891908
	Σ complexity	**4314995**	**4315458**	**4936885**	**270622223**	**22753217**
	Complexity (normalized)	**0.015945**	**0.015946**	**0.018243**	**1**	**0.084077**
Rayleigh & AWGN	Reciver (multiplication)	445036	445037	547948	35323	2905103
	Reciver (addition)	1708020	1707615	1989336	786837	9036203
	Σ multiplication	1189881	1190055	1396226	44624666	5861509
	Σ addition	3290315	3290604	3782560	226164558	17506909
	Σ complexity	**4480196**	**4480659**	**5178786**	**270789224**	**23368418**
	Complexity (normalized)	**0.016545**	**0.016547**	**0.019125**	**1**	**0.086297**
Rician & AWGN	Reciver (multiplication)	445036	445037	547948	35323	2905103
	Reciver (addition)	1708020	1707615	1989336	786837	9036203
	Σ multiplication	1189881	1190055	1396226	44624666	5861509
	Σ addition	3290315	3290604	3782560	226164558	17506909
	Σ complexity	**4480196**	**4480659**	**5178786**	**270789224**	**23368418**
	Complexity (normalized)	**0.016545**	**0.016547**	**0.019125**	**1**	**0.086297**

Table 5: *Comparative Study on the Modulation Schemes.*

Metrics	CP-OFDM	W-OFDM	F-OFDM	UFMC	FBMC
filter or window used	N/A	raised cosine window	Sinc function with Hanning window in time-domain	Dolph-Chebyshev filter in time-domain	Phydyas filter in time-domain
filtering method	N/A	N/A	the whole band altogether	per subband	per subcarrier
filter or window length	N/A	same as the overlap of prefix and suffix	exceeds CP	equal to CP	K times subcarrier
orthogonality	preserved	preserved	slightly lost	preserved	preserved
PAPR	high	high	highest	higher	higher
CCDF of PAPR	high	high	higher	higher	highest
BER	low	low	lower	lower	lowest
roll-off rate	low	high	higher	high	highest
spectral leakage	highest	higher	low	high	lowest
spectral efficiency	low	high	higher	high	highest
computational complexity	high	high	high	highest	higher
runtime complexity	low	low	higher	high	highest

balance is achieved through much higher computational complexity. For this reason, UFMC acts as a halfway approach from CP-OFDM towards FBMC.

In brief, FBMC is the preferred scheme for efficient spectrum usage. If transmission accuracy is a higher priority, F-OFDM may be preferred since FBMC does not use CP. W-OFDM gives a lower PAPR value close to CP-OFDM. Finally, UFMC creates a delicate balance among the performance metrics conceding high computational complexity.

ACKNOWLEDGMENT

The research reported in this paper was carried out at the Budapest University of Technology and Economics and it has been supported by the National Research, Development, and Innovation Fund of Hungary under Grant TKP2021-EGA-02.

References

[1] H. Jebbar, S. E. Hassani and A. E. Abbassi, "Performance study of 5G multicarrier waveforms," *2017 International Conference on Wireless Networks and Mobile Communications (WINCOM)*, pp. 1-6, 2017.

[2] A. Hazareena and B.A. Mustafa, "A survey: On the waveforms for 5G," in *2018 Second International Conference on Electronics, Communication and Aerospace Technology (ICECA)*, pp. 64-67, 2018.

[3] M. Van Eeckhaute, A. Bourdoux, P. De Doncker and F. Horlin, "Performance of emerging multi carrier waveforms for 5G asynchronous communications," *EURASIP Journal on wireless communications and networking*, no. 29, pp. 1-15, 2017.

[4] F. Schaich and T. Wild, "Waveform contenders for 5G — OFDM vs. FBMC vs. UFMC," *2014 6th International Symposium on Communications, Control and Signal Processing (ISCCSP)*, pp. 457-460, 2014.

[5] A.S. Rachini and M.M. Jaber, "Performance of FBMC in 5G mobile communications over different modulation techniques," in *2019 Interna-*

tional Symposium on Networks, Computers and Communications (ISNCC), pp. 1-6 , 2019.

[6] R. Gerzaguet, N. Bartzoudis, L.G. Baltar, V. Berg, J.B. Doré, D. Kténas, O. Font-Bach, X. Mestre, M. Payaró, M. Färber and K. Roth, "The 5G candidate waveform race: a comparison of complexity and performance," *EURASIP Journal on Wireless Communications and Networking*, no. 13, pp.1-14, 2017.

[7] G.H. Geleta, D.M. Molla and K.A.Fante, "Comparative Study of Modulation Techniques for 5G Networks," in *International Conference on Advances of Science and Technology*, vol. 274, pp. 503-518, Springer, Cham., 2018.

[8] K. Choi, "FD-FBMC: A Solution for Multicarrier Full Duplex Cellular Systems," in *IEEE Communications Letters*, vol. 25, no. 2, pp. 617-621, Feb. 2021

[9] A. Hammoodi, L. Audah and M. A. Taher, "Green Coexistence for 5G Waveform Candidates: A Review," in *IEEE Access*, vol. 7, pp. 10103-10126, 2019.

[10] B. Rashmi, and K. Saraswathi, "Performance Analysis of OFDM, FBMC and UFMC Modulation Schemes for 5G Mobile Communication MIMO systems," *Proceedings of the International Conference on IoT Based Control Networks & Intelligent Systems - ICICNIS 2021.*, 2021.

[11] X. Wendi, Y. Lin and W. Jing, "Research of Several Multicarrier Transmission Technologies in Mobile Communication," in *Journal of Physics: Conference Series*, vol. 1314, no. 1, pp. 012205, IOP Publishing, 2019.

[12] R.N. Youngworth, B.B.Gallagher and B.L. Stamper, "An overview of power spectral density (PSD) calculations," in *Optical Manufacturing and Testing VI*, vol. 5869, pp. 58690U, 2005.

[13] G. Gritsch, H. Weinrichter and M. Rupp, "A union bound of the bit error ratio for data transmission over correlated wireless MIMO channels," *2004 IEEE International Conference on Acoustics, Speech, and Signal Processing*, pp. iv-iv, 2004.

[14] V. Tarokh and H. Jafarkhani, "On the computation and reduction of the peak-to-average power ratio in multicarrier communications," in *IEEE Transactions on Communications*, vol. 48, no. 1, pp. 37-44, Jan. 2000.

[15] J.C. Helton and H.J. Iuzzolino, Construction of complementary cumulative distribution functions for comparison with the EPA release limits for radioactive waste disposal. Reliability Engineering & System Safety, 40(3), pp.277-293.1993.

[16] A. B. Awoseyila, C. Kasparis and B. G. Evans, "Robust time-domain timing and frequency synchronization for OFDM systems," in *IEEE Transactions on Consumer Electronics*, vol. 55, no. 2, pp. 391-399, May 2009.

[17] W. Henkel, G. Taubock, P. Odling, P.O. Borjesson and N. Petersson, "The cyclic prefix of OFDM/DMT-an analysis," in *2002 International Zurich Seminar on Broadband Communications Access-Transmission-Networking (Cat. No. 02TH8599)*, pp. 22-22, 2002.

[18] L. Litwin and M. Pugel, "The principles of OFDM," *RF signal processing*, vol. 2, pp. 30-48, 2001.

[19] C. RoBing and V. Tarokh, "A construction of OFDM 16-QAM sequences having low peak powers," in *IEEE Transactions on Information Theory*, vol. 47, no. 5, pp. 2091-2094, July 2001.

[20] B. Muquet, Zhengdao Wang, G. B. Giannakis, M. de Courville and P. Duhamel, "Cyclic prefixing or zero padding for wireless multicarrier transmissions?," in *IEEE Transactions on Communications*, vol. 50, no. 12, pp. 2136-2148, Dec. 2002

[21] A. Zaidi, F. Athley, J. Medbo, U. Gustavsson, G. Durisi and X. Chen, "5G Physical Layer," *principles, models and technology components*, Academic Press, 2018.

[22] Y. Ding, T. N. Davidson, Zhi-Quan Luo and Kon Max Wong, "Minimum BER block precoders for zero-forcing equalization," in *IEEE Transactions on Signal Processing*, vol. 51, no. 9, pp. 2410-2423, Sept. 2003.

[23] A. Tarighat and A. H. Sayed, "An optimum OFDM receiver exploiting cyclic prefix for improved data estimation," *2003 IEEE International Conference on Acoustics, Speech, and Signal Processing, 2003. Proceedings. (ICASSP '03).*, pp. IV-217, 2003.

[24] H. A. Mahmoud and H. Arslan, "Sidelobe suppression in OFDM-based spectrum sharing systems using adaptive symbol transition," in *IEEE Communications Letters*, vol. 12, no. 2, pp. 133-135, February 2008.

[25] K. Mizutani, T. Matsumura and H. Harada, "A comprehensive study of universal time-domain windowed OFDM-based LTE downlink system," *2017 20th International Symposium on Wireless Personal Multimedia Communications (WPMC)*, pp. 28-34, 2017.

[26] C. Muschallik, "Improving an OFDM reception using an adaptive Nyquist windowing," *IEEE transactions on Consumer Electronics*, vol. 42, no. 3, pp.259-269, 1996.

[27] H. Kim, I. Jung, Y. Park, W. Chung, S. Choi and D. Hong, "Time Spread-Windowed OFDM for Spectral Efficiency Improvement," in *IEEE Wireless Communications Letters*, vol. 7, no. 5, pp. 696-699, Oct. 2018.

[28] Y. Mizutani, K. Mizutani, T. Matsumura and H. Harada, "A Low Pass Filtered-Raised-Cosine Window for UTW-DFTs-OFDM," *2018 21st In-*

ternational Symposium on Wireless Personal Multimedia Communications (WPMC), pp. 641-646, 2018.

[29] D. Mattera and M. Tanda, "Windowed OFDM for small-cell 5G uplink," *Physical Communication*, vol. 39, pp. 100993, 2020.

[30] A. Cortes, I. Velez, J. F. Sevillano and A. Irizar, "An approach to simplify the design of IFFT/FFT cores for OFDM systems," in *IEEE Transactions on Consumer Electronics*, vol. 52, no. 1, pp. 26-32, Feb. 2006

[31] B. Peköz, Z. E. Ankaralı, S. Köse and H. Arslan, "Non-Redundant OFDM Receiver Windowing for 5G Frames and Beyond," in *IEEE Transactions on Vehicular Technology*, vol. 69, no. 1, pp. 676-684, Jan. 2020

[32] J. Abdoli, M. Jia and J. Ma, "Filtered OFDM: A new waveform for future wireless systems," *2015 IEEE 16th International Workshop on Signal Processing Advances in Wireless Communications (SPAWC)*, pp. 66-70, 2015.

[33] H. Huawei, "F-OFDM scheme and filter design," in *Proceedings of the 3GPP TSG RAN WG1 Meeting*, vol. 85, pp. R1-165425), 2016.

[34] P. Podder, T.Z. Khan, M.H. Khan and M.M. Rahman, "Comparative performance analysis of hamming, hanning and blackman window," *International Journal of Computer Applications*, vol. 96, no. 18, 2014.

[35] H. Huawei, "OFDM based flexible waveform for 5G," in *R1-162152, 3GPP TSG RAN WG1 meeting 84bis*, 2016.

[36] T. Wild, F. Schaich and Y. Chen, "5G air interface design based on Universal Filtered (UF-)OFDM," *2014 19th International Conference on Digital Signal Processing*, pp. 699-704, 20140.

[37] K. Xu, "The Chebyshev points of the first kind," *Applied Numerical Mathematics*, vol. 102, pp. 17-30, 2016.

[38] F. Schaich, T. Wild and Y. Chen, "Waveform Contenders for 5G - Suitability for Short Packet and Low Latency Transmissions," *2014 IEEE 79th Vehicular Technology Conference (VTC Spring)*, pp. 1-5, 2014.

[39] B. Farhang-Boroujeny, "OFDM Versus Filter Bank Multicarrier," in *IEEE Signal Processing Magazine*, vol. 28, no. 3, pp. 92-112, May 2011.

[40] M. Schellmann et al., "FBMC-based air interface for 5G mobile: Challenges and proposed solutions," *2014 9th International Conference on Cognitive Radio Oriented Wireless Networks and Communications (CROWNCOM)*, pp. 102-107, 2014.

[41] M. Bellanger, D. Le Ruyet, D. Roviras, M. Terré, J. Nossek, L. Baltar, Q. Bai, D. Waldhauser, M. Renfors, and T. Ihalainen, "FBMC physical layer: a primer," *Phydyas*, vol. 25, no. 4, pp. 7-10, 2010.

[42] T. Jiang, D. Chen, C. Ni and D. Qu, "OQAM/FBMC for future wireless communications," *Principles, technologies and applications*, Academic Press, 2017.

[43] M. Carvalho, M. L. Ferreira and J. C. Ferreira, "FPGA-based implementation of a frequency spreading FBMC-OQAM baseband modulator," *2017 24th IEEE International Conference on Electronics, Circuits and Systems (ICECS)*, pp. 174-177, 2017.

[44] M. Bellanger, "FS-FBMC: An alternative scheme for filter bank based multicarrier transmission," *2012 5th International Symposium on Communications, Control and Signal Processing*, pp. 1-4, 2012.

[45] G. Wunder et al., "5GNOW: Intermediate frame structure and transceiver concepts," *2014 IEEE Globecom Workshops (GC Wkshps)*, pp. 565-570, 2014.

[46] S. Thota, Y. Kamatham and C. S. Paidimarry, "Analysis of Hybrid PAPR Reduction Methods of OFDM Signal for HPA Models in Wireless Communications," in *IEEE Access*, vol. 8, pp. 22780-22791, 2020.

[47] S. Kutty and D. Sen, "Beamforming for Millimeter Wave Communications: An Inclusive Survey," in *IEEE Communications Surveys & Tutorials*, vol. 18, no. 2, pp. 949-973, Secondquarter 2016.

Abu Shakil Ahmed is studying towards a Ph.D. degree in Electrical Engineering at University College Dublin, Ireland. He received an MSc degree in 2021 from Budapest University of Technology and Economics, Hungary, and a BSc degree in 2018 from Khulna University of Engineering & Technology, Bangladesh. After graduation, he served as a Lecturer at Leading University, Bangladesh from 2018 to 2019.

Husam AL-amaireh received his Ph.D. degree in Electric Engineering from the Budapest University of Technology and Economics in 2021. He was a member of BME MATLAB Laboratory. His research interests are digital signal processing, FBMC, massive MIMO, and wireless communications.

Zsolt Kollár was born in 1983. He received his Ph.D. degree in Electric Engineering from the Budapest University of Technology and Economics in 2013. He is currently an associate professor in the Department of Measurement and Information Systems. Since 2016, he is the head of the MATLAB Laboratory. His research interests include digital signal processing, quantization effects and wireless communication.